# Comparing Different Potential Flow Methods for Unsteady Aerodynamic Modelling of a Flutter Demonstrator Aircraft

Thiemo M. Kier *

*DLR (German Aerospace Center), Institute of System Dynamics and Control, 82234 Weßling, Germany*

**To further improve the performance of aircraft, the aspect ratios in recent designs grow larger. However, the resulting increased flexibility of the wings might have a detrimental effect on the flutter stability of the aerostructural system. Apart from structural changes that have a negative impact on the weight of the airframe, an Active Flutter Suppression (AFS) system can be employed to prevent such instabilities within the flight envelope.**

**To develop these AFS control laws, accurate simulation and synthesis models of the flexible airframe are essential. Still today, the workhorse for modelling unsteady compressible aerodynamics for such models is the Doublet Lattice Method (DLM). However, there are some shortcomings regarding this method. One particular point is the absence of in-plane forces, which are essential for phenomena such as T-tail flutter. Also low frequency in-plane modes that might change the flutter mechanism for aircraft with high AR wings, can not be accurately modelled by the standard DLM. To address this issue, other unsteady aerodynamic methods based on potential flow are employed and compared to the standard DLM results.**

**The DLM can be extended to include forces in x-direction. This enhanced formulation requires a modification of the boundary conditions at the box quarter chord points to recover complex directional lift forces as function of the reduced frequency. Alternatively, the unsteady 3D panel method USNEWPAN can be employed, which is based on the velocity potential and features thickness effects of the airfoil. The pressure integration over the contour then captures the in-plane forces. The solver USNEWPAN is similarly to the DLM, a compressible frequency domain method, which can also produce so called Aerodynamic Influence Coefficient (AIC) matrices that relate normal velocities at the collocation points to pressures.**

**Complex valued Generalized Aerodynamic Forces (GAFs) are obtained using the normal modes of the aircraft structure and the corresponding differentiation matrices. These GAF matrices of the different aerodynamic methods are then used in subsequent flutter calculations.**

## I. Introduction

Future aircraft concepts show a significant increase of the wing span, as high aspect ratio planforms promise a substantial reduction of the induced drag. However, such high aspect ratio wings become more flexible and might have detrimental effects on the controllability, performance and the flutter stability of the airframe. Apart from structural modifications with its weight penalties, active control methods offer a way to address these issues. Wing Shape Control can optimize the drag during the mission in off-design flight conditions[1], Active Gust and Manoeuvre Load Alleviation (GLA and MLA) functions can reduce the design loads and therefore reduce the structural weight[2, 3, 4], and an Active Flutter Suppression (AFS) Control System[5] can prevent aeroelastic instabilities within the flight envelope.

The EU projects FLEXOP (Flutter Free FLight Envelope eXpansion for ecOnomic Performance improvement) and its successor FLiPASED (Flight Phase Adaptive Aero-Servo-Elastic Aircraft Design Methods) aim to advance methods for active control technologies of flexible aircraft in early design phases. During the projects a subscale demonstrator aircraft named T-FLEX was build to test these active control technologies in flight [6]. The aircraft has a span of 7 m and weighs 65 kg. A set of wings was designed to feature an intentional flutter behavior within the operating envelope of the demonstrator. The outboard ailerons are equipped with high bandwidth actuators, which can be used to stabilize the aeroelastic instability with active flutter suppression (AFS) control laws.

For the model based design methodologies of control theory for the AFS, fast, yet accurate modelling of the airframe is required. A mathematical model of the demonstrator aircraft has been developed [7] based on the integrated modelling framework [8, 9] developed at the DLR Institute of System Dynamics and Control. Based on the previously described model, control laws for an AFS have been designed. The synthesis methods are described in detail in the

*Research Scientist, Department of Aircraft Systems Dynamics, Thiemo.Kier@dlr.de

references [5, 10, 11]. Since the control Laws are to be flown on the demonstrator, precise flutter predictions and synthesis models are required.

The aerodynamic used for the nominal model is the standard Doublet Lattice Method (DLM) [12, 13, 14]. This method has some shortcomings as it can not account for lift forces due to in-plane motion of the lifting surfaces. To address this issue, an enhanced DLM method was implemented and compared to the standard DLM results.

To accurately account for the directional lift, the standard DLM can be enhanced by using the cross product form of the Kutta-Joukowsky Law instead of merely a scalar multiplication. The resulting boundary conditions can be expressed in matrix form as described in [1]. The derivation follows largely the method described by van Zyl [15, 16]. The enhanced DLM also features a source panel representation of fuselage like components. This implementation necessitates the implementation of the unsteady backwash kernel in addition to the planar and nonplanar terms of the normalwash. This backwash is required to account for the changes in onflow direction in the case of the wing surfaces, as well as the body panels with normal vectors that have a component in x-direction.

Furthermore, the unsteady 3D panel method USNEWPAN [17, 18] has been used to model the demonstrator aircraft. USNEWPAN is based on the velocity potential and models the surface contour of the wings and is therefore able to account for the thickness of the wings. The in-plane forcing is then recovered by pressure integration along the actual wing surface.

For comparison of the aerodynamic methods, three different aerodynamic grid were created. The first includes only the lifting surfaces, the second models the fuselage with cruciform shaped lifting surfaces, and the third accounts for the fuselage by nonlifting body source panels of the actual surface. These grids were used to assess the influence of the different modelling strategies of the fuselage.

Flutter analyses were performed for the standard DLM as well as its enhanced counterpart (eDLM). The results were obtained by a standard frequency domain iterative $p-k$ method, as well as a $p$ method.The p method reuires a Rational function approximation of the frequency dependent Generalized Aerodynamic Force (GAF) matrices to make them amenable for a state space representation of the aeroelastic system.

Further investigations concern the influence of the aerodynamic methods on the in plane structural GAFs. The influence of the fuselage modelling strategies were assessed by examining the GAFs for the rigid body modes. Finally, a 3D panel method based on the velocity potential is used to model the surface contour of the wings. The GAFs of this fourth model were compared for the flutter relevant aerodynamic forces.

# II. Aerodynamic Methods

First some remarks about the theory and implementation aspects of the aerodynamic methods are presented.

## A. Governing Flow Equations

The governing flow equations for the panel method as well as the DLM are the unsteady linearized potential flow equations, sometimes also referred to as the unsteady Prandtl-Glauert equations. The derivation of methods based on potential flow starts out with the steady velocity potential $\Phi_S$.

$$\left(1-M_\infty^2\right)\frac{\partial^2\Phi_S}{\partial x^2}+\frac{\partial^2\Phi_S}{\partial y^2}+\frac{\partial^2\Phi_S}{\partial z^2}=0 \tag{1}$$

Using a Göthert Type 2 transformation [19], the problem can be reduced to a Laplace type equation $\nabla^2\Phi_S=0$.

Equation (1) covers quasisteady aerodynamics at a given instance in time. The circulation around the flow field can be calculated by the closed contour integral $\Gamma=\oint V\cdot\mathrm{d}s$. The lift per unit span is directly related to the circulation via the Kutta Joukowsky Law $L'=\rho_\infty U_\infty \Gamma$. However, when the normalwash of a lifting surface varies, the overall circulation changes. Kelvin's theorem states that this overall circulation within a control volume must remain constant over time.

$$\frac{\mathrm{d}\Gamma}{\mathrm{d}t}=0 \tag{2}$$

Therefore, when the circulation of the airfoil changes due to the tangential flow boundary condition, vorticity of equal strength but opposite sign has to be generated. For an attached flow, this vorticity is shed at the trailing edge and subsequently convected downstream with $U_\infty$, forming a wake vortex sheet with strength $\gamma_w$. For slow changes of the normal wash, the influence of shed vorticity in the wake on the airfoil is negligible. If at each time step the normal wash is varied to account for motion of the airfoil, but the effects of the shed vortices are neglected, this is the so called quasi-steady approximation. For fast changing velocities which occur e.g. in gust loads or flutter analysis this approximation no longer holds and the modelling of the unsteady aerodynamics is essential.

If furthermore the unsteady flow is compressible, the pressure disturbances propagate with a finite speed of sound $a_\infty$, whereas in the incompressible case, the lagging behavior is purely confined to the convection of the wake. For compressible flow these propagating pressure waves add another cause for time dependence, which is reflected by the presence of the partial derivatives wrt to time in the unsteady Prandtl-Glauert equation.

$$\left(1 - Ma_\infty^2\right) \frac{\partial^2 \Phi_U}{\partial x^2} + \frac{\partial^2 \Phi_U}{\partial y^2} + \frac{\partial^2 \Phi_U}{\partial z^2} - \left(2\frac{Ma_\infty}{a_\infty}\right) \frac{\partial^2 \Phi_U}{\partial x \partial t} - \left(\frac{1}{a_\infty^2}\right) \frac{\partial^2 \Phi_U}{\partial t^2} = 0 \tag{3}$$

The unsteady Prandtl-Glauert equation (3) can be subjected to the following transformation:

$$\Phi_U(x, y, z, t) = \varphi_U(X, Y, Z) \cdot \exp\left(\mathrm{j}k\frac{Ma^2}{1 - Ma^2}X + k\tau\right), \tag{4}$$

which yields as result the Helmholtz equation

$$\nabla^2 \varphi_U + \kappa^2 \varphi_U = 0, \quad \text{with} \quad \kappa = k\frac{Ma}{1 - Ma^2}, \tag{5}$$

which is indicative of the wave like behavior. For steady ($k = 0$) or incompressible ($Ma = 0$) flow, the problem reduces to the Laplace equation $\nabla^2 \varphi = 0$.

## B. steady Vortex Lattice Method

The Vortex Lattice Method (VLM) solves the steady velocity potential equation (1) by discretizing the mean lifting surface by so called horseshoe vortices, where the bound vortex lies on the quarter chord of each box and the trailing vortices extend to infinity. According to the Helmholtz theorems, such a vortex must either end at a solid surface, or extend to infinity. Hence, the bound vortex is extended at both corner points to infinity, forming the well known horseshoe shape with its legs pointing in free stream direction. The circulation strengths $\mathbf{\Gamma}_j$ of the individual horseshoe vortices are then determined by the Biot-Savart-Law and by meeting the flow compatibility condition, i.e. no perpendicular flow $\mathbf{v}_j$ through the solid surface at the control points at $3/4$ chord, according to Pistolesi's theorem [20].

The load acting point is located at mid span, quarter chord ($l-\text{set}$) and the control point at three quarter ($j-\text{set}$) chord point, respectively. The box reference point ($k-\text{set}$) is at the center of the box. The panel chord is $c_j$ and the span is $b_j$. The vector of the bound vortex is denoted by $\mathbf{b}_l$.

The Kutta-Joukowski-Law can be cast in a form, involving a cross product to account for a directional lift vector. This approach was detailed for an enhanced Vortex Lattice Method in [1] to account for induced drag in the analysis of flexible aircraft. A simple scalar multiplication instead of the cross product greatly simplifies the analysis, however results merely in a scalar lift quantity in z-direction.

$$\mathbf{L}_l = \rho \mathbf{V}_l \times (\mathbf{b}_l \Gamma_j) \qquad \text{with} \;\; \mathbf{L}_l, \mathbf{V}_l, \mathbf{b}_l \in \mathbb{R}^3 \;\; \text{and} \;\; \Gamma_j \in \mathbb{R}^1 \tag{6}$$

The vector $\mathbf{b}_l$ is the vector quantity between the two corners of the horseshoe vortex, i.e. the bound vortex. The lift force $\mathbf{L}_l$ then acts, as aerodynamic theory predicts, perpendicular to the local stream velocity $\mathbf{V}_l$ at the quarter chord point.

Equation (6) can now be recast in matrix form by using the skew matrix operator $\mathbf{sk}()$ for the cross product.

$$\mathbf{L}_l = q_\infty \left(\Big[-\mathbf{sk}(\mathbf{b}_l)\Big]\mathbf{w}_l\right) \odot \left(c_j \begin{bmatrix}1 & 1 & 1\end{bmatrix}^{\mathrm{T}} \Delta c_{p_j}\right) \tag{7}$$

The vector $\mathbf{w}_l$ is the velocity at quarter chord normalized by the free stream velocity. The operator $\odot$ in eq. (7) refers to an elementwise multiplication. Since both $\mathbf{w}_l$, as well as $\mathbf{w}_j$ (respectively $\Delta c_{p_j}$) depend on the boundary conditions, expression (7) is inherently nonlinear. Therefore, it is computationally more expensive compared to the linear expression in scalar form of the Kutta-Joukowsky Law. If $\mathbf{w}_l = \begin{bmatrix}1 & 0 & 0\end{bmatrix}^{\mathrm{T}}$, i.e. the free stream is assumed to be exclusively in x-direction, the analysis simplifies to the conventional case, with the lift $\mathbf{L}_l$ acting in the z-direction only.

In a last step, the lift vector $\mathbf{L}_l$ at the quarter chord is transformed to the reference point at the aerodynamic box centroid.

$$\mathbf{P}_k^{\text{aero}} = \mathbf{T}_{lk}^{\mathrm{T}}\, \mathbf{L}_l \tag{8}$$

### C. Doublet Lattice Method

The Doublet Lattice Method [12, 13, 14] (DLM) provides a harmonic solution for the unsteady Prandtl-Glauert equation (3). Furthermore, it uses the acceleration potential. Since the acceleration potential is formally equivalent to the velocity potential equation, the same elementary solutions are valid, e.g. the source potential. Analog to acoustics, the harmonically oscillating source is moved wrt a resting fluid, followed by a Gallilei transformation, which moves the observer with the source. Lift can not be generated by a source, hence the source potential is differentiated in the z-direction, leading to the doublet potential. The acceleration potential directly yields the pressure difference between the upper and lower surface, which makes additional steps, i.e. the use of the Kutta-Joukowsky Law, in the load recovery process unnecessary. However, the acceleration potential of the doublet still needs to be integrated to calculate the induced velocity, which is needed to meet the flow tangency condition on the lifting surface. Contrary to the velocity potential of a free flying wing, where there is a velocity discontinuity across the wake surface, there is no such discontinuity in the pressure, hence the wake needs not to be modelled for acceleration potential methods.

The DLM is the unsteady extension to the VLM, which similarly places the singularity along the quarter chord and satisfies the flow tangency at the three quarter chord. The doublet potential is evaluated at discrete points along the quarter chord line, which are used for a polynomial fit and its subsequent analytical integration. The integration still can not be performed in closed form and series approximations for parts of the kernel functions need to be employed. The final result for the pressure coefficient

$$\Delta \mathbf{c_p}_j(k) = \mathbf{Q}_{jj}(k)\mathbf{w}_j(k) \tag{9}$$

has similar form to the conventional steady aerodynamics, where

$$k = \tfrac{c_{\mathrm{ref}}/2}{U_\infty}\omega \tag{10}$$

is the reduced frequency. For $k = 0$ the DLM solution is replaced with the VLM results [21], since for the steady case no approximations are required.

### D. enhanced Doublet Lattice Method

Similarly to the Vortex Lattice Method, the Kutta-Joukowsky Law can be applied in its vector form (6) to the pressure coefficients (9) from the DLM . This way the an unsteady directional lift vector can be computed. This approach has been suggested by van Zyl [15, 16] in the context of T-tail flutter. The enhanced eDLM correctly reflects the onflow condition at the quarter chord point by considering the motion induced velocities via the boundary condition matrices. Furthermore, the induced in-plane velocities need to be considered by implementing the backwash kernel. This is done either with the method proposed by van Zyl in [15] or the one Rodden formulated in [21]. The boundary conditions of the present enhanced Doublet Lattice Method (eDLM) are computed with differentiation matrices, which are described in a subsequent section.

Furthermore, nonlifting bodies can be modelled by source panels similar to the 3D velocity potential method in the next section. The unsteady implementation follows the derivation of Kirkup [22] for the Helmholtz kernel evaluation by Gaussian integration of a quadrilateral unsteady source panel and combined with the potential generated by the acceleration doublet singularities of the DLM. Such an extension was also already suggested by van Zyl in [15].

### E. unsteady 3D Panel Method

In the case of the 3D panel method the actual and not the mean surface is discretized. The basic solutions chosen are velocity potential source and doublet panels. The result is a velocity potential distribution. Differentiation of this velocity potential in the spatial directions yield the flow velocities on the surface, which in turn can be used to determine the surface pressures and ultimately the lifting forces for the steady case.

The steady solution of a, possibly deformed reference shape, defines the flight state about which an unsteady linearization is performed. The unsteady solution is then found by solving the linearized frequency domain variant of the unsteady Prandtl-Glauert equation, respectively the Helmholtz equation $\nabla^2\Phi_U + \kappa^2\Phi_U = 0$. Note that $\kappa$ is a frequency parameter depending on the reduced frequency $k = \frac{c_{\mathrm{ref}}/2}{U_\infty}\omega$ and Mach number. The total velocity potential is then

$$\Phi(x, y, z, \omega) = \Phi_S(x, y, z) \;+\; \mathrm{e}^{\mathrm{j}\omega t}\;\Phi_U(x, y, z), \tag{11}$$

where $\Phi_U$ is the unsteady perturbation potential.

In the case of the unsteady panel method, this expression is used to calculate the complex unsteady pressure via a linearized version of the unsteady Bernoulli equation. The coupling between the steady and unsteady flow is accounted for by the 3D panel method intrinsically.

### F. Aerodynamic Influence Coefficient Matrices and Boundary Conditions

The previously described aerodynamic methods have in common the concept of the frequency dependent Aerodynamic Influence Coefficient (AIC) matrix. The AIC matrix relates a normal wash at a control point to a pressure at each of the discretization elements for discrete harmonic excitations in the frequency domain. When calculated over a range of reduced frequencies $k$, transfer functions relating normal wash excitations to pressures can be determined.

The perturbation pressures $\Delta\,\mathbf{c_p}$ about the steady state can be calculated with the following equation:

$$\mathbf{c_p}_j(k) = \left[\mathbf{Q}_{jj}\ \left(\mathbf{D^x}_{jk} + \mathrm{j}k\cdot\ \mathbf{D^t}_{jk}\right)\ + \left(\mathbf{DP^x}_{jk} + \mathrm{j}k\cdot\ \mathbf{DP^t}_{jk}\right)\right]\ \mathbf{u}_k(k), \tag{12}$$

where the matrix $\mathbf{D^x}_{jk}$ accounts for a change in downwash due to a change of the normal vector with respect to the free stream direction and the matrix $\mathbf{D^t}_{jk}$ for additional downwash due to movement of the boundary in direction of the panel normal.

$$\mathbf{w}_j = \left(\mathbf{D^x}_{jk}\ + \mathrm{j}k\cdot\ \mathbf{D^t}_{jk}\right)\cdot\mathbf{u}_k(k) \tag{13}$$

When thick bodies are modeled in potential flow, additional pressure contributions arise. These are not associated with the normalwash, but with tangential flow at the panels. Therefore, the 3D Panel Method, requires the additional motion induced terms $\mathbf{DP^x}_{jk}$ and $\mathbf{DP^t}_{jk}$. It should be noted that these terms are dependent on the onflow direction, i.e. they are associated with the flight state, about which the AIC was linearized. For thin velocity potential panels as well as in the DLM these terms are zero.

To make use of the vector form of the Kutta-Joukowsky Law (7), the onflow also has to be determined in vector form. The differentiation matrix $\mathbf{D^t}_{lk}$ is therefore set up equivalently for the three translational DOFs at the quarter chord to determine the contribution of the flexible motion.

$$\mathbf{w}_l = \mathrm{j}k\cdot\ \mathbf{D^t}_{lk}\cdot\mathbf{u}_k(k) \tag{14}$$

This motion induced value for $\mathbf{w}_l$ then needs to be augmented with the free stream velocity vector and the induced velocities of the singularity distributions. The vector $\mathbf{u}_k(k)$ describes the motion of the individual panels at their reference point, which may result from rigid body motion, flexible deformation or control surface deflections.

### G. Generalized Aerodynamic Forces

The load transformation to panel reference point is done by integrating the pressures $\mathbf{c_p}_j$. For the 3D panel method, where the box reference $k$, force application $l$ and collocation $j$ points coincide, the pressure coefficients are simply multiplied with the box area. For the DLM, aditionally an offset between force application location and the panel reference point is present. The respective moment arms are accounted for by the integration matrix $\mathbf{S}_{kj}$, if rotational degrees of freedom are introduced in the aerodynamic $(k - set)$. The aerodynamic loads have to be mapped to the structural degrees of freedom. The matrix connecting the displacements of the structural grid $(g - set)$ to the aerodynamic grid $(k - set)$ is called spline matrix $\mathbf{T}_{kg}$. Finally, the eigenvector matrix $\mathbf{\Phi}_{gh}$ of the normal modes analysis of the structure is used to obtain the Generalized Aerodynamic Forces (GAF):

$$\mathbf{Q}_{hh}(k) = \mathbf{\Phi}_{gh}^{\mathrm{T}}\ \mathbf{T}_{kg}^{\mathrm{T}}\ \mathbf{S}_{kj}\ \left[\mathbf{Q}_{jj}\ \left(\mathbf{D^x}_{jk} + \mathrm{j}k\cdot\ \mathbf{D^t}_{jk}\right)\ + \left(\mathbf{DP^x}_{jk} + \mathrm{j}k\cdot\ \mathbf{DP^t}_{jk}\right)\right]\ \mathbf{T}_{kg}\ \mathbf{\Phi}_{gh} \tag{15}$$

In the case of the cross product version, the directional lift vector $\mathbf{L}_l$ is determined from the onflow velocity $\mathbf{w}_l$ and the pressure coefficients $\Delta\mathbf{c_p}_j(k)$. With eq. (8), the GAF matrix $\mathbf{Q}_{hh}$ can be assembled accordingly including the directional terms for the velocity. It should be emphasized that in this case the GAF matrix depends on the steady loading.

After multiplication with the dynamic pressure, the GAF matrices can be inserted in the linear equations of motion, representing the flutter equation analyzed with respect to stability.

$$\left(-\omega^2\mathbf{M}_{hh} + \mathrm{j}\omega\mathbf{B}_{hh} + \mathbf{K}_{hh} - q_\infty\mathbf{Q}_{hh}(k)\right)\mathbf{u}_h = 0 \tag{16}$$

The flutter equation is examined for unstable poles, when the flight velocity is increased. The flutter problem can be solved in the frequency domain using the $p-k$ method. Alternatively, the GAF matrices can be fitted with a regression using a so called Rational Function Approximation (RFA). Subsequently the problem can be cast in state space form and a simple eigenvalue problem of the system matrix yields the poles of the aeroelastic problem. This is the so called $p$ method.

# III. Structural Dynamics of the Flutter Demonstrator

The structural properties of the T-FLEX aircraft have been modelled using a Finite Element Model (FEM) of the flutter wings attached to the fuselage as described in [23]. To reduce the number of Degrees of Freedom (DoF) a static condensation to a reference axis system, a so called Guyan reduction [24] is applied. For the following flutter analysis the eigenvalues and eigenvectors are determined by a normal modes analysis of the FE model in free-free configuration. To assure that the structural dynamic properties are preserved after the condensation process a comparison between the shapes and frequencies of the condensed and full model was done [23]. The first six eigenvalues of the free-free boundary condition are zero. The associated rigid body eigenvectors are determined geometrically about the center of gravity in body fixed axes directions compatible with the flight mechanical coordinate system.

Table 1 lists and describes the first six flexible modes and their associated frequencies.

**Table 1. flexible eigenmodes of the flutter demonstrator aircraft**

| mode number | description | frequency [Hz] |
|---|---|---|
| 7 | symmetric – 1st wing bending | 2.92 |
| 8 | antisymmetric – 1st wing bending | 8.16 |
| 9 | symmetric – 1st wing torsion | 10.50 |
| 10 | antisymmetric – 1st wing torsion | 10.61 |
| 11 | symmetric – 2nd wing bending | 12.13 |
| 12 | symmetric – 1st wing in-plane bending | 15.06 |

These are the modes that participate in the two flutter mechanisms that are discussed later. The associated mode-shapes of the first six flexible modes are depicted in figure 1

# IV. Flutter Analysis

## A. $p-k$ Method

The $p-k$ method, or "British"-method, is a frequency domain method, which was formulated by Hassig [25]. It is one of the classical frequency domain methods, implemented in many standard aeroelastic flutter tools [26]. The equation to be solved by the $p-k$ method is

$$\left[\mathbf{M}_{hh}\, p^2 + \left(\mathbf{B}_{hh} - q_\infty \frac{c_{ref}/2}{V}\, \mathrm{Im}\left(\mathbf{Q}_{hh}(k)\right) \frac{1}{k}\right) p + \left(\mathbf{K}_{hh} - q_\infty\, \mathrm{Re}\left(\mathbf{Q}_{hh}(k)\right)\right)\right] \mathbf{u_h} = 0. \tag{17}$$

The generalized aerodynamic forces are split into a damping and a stiffness part and subtracted from its structural counterparts accordingly. Since the eigenvalue $p$ is not independent from the reduced frequency $k$, the eigenvalues have to be determined iteratively.

$$k = \frac{c_{ref}/2}{V}\, \mathrm{Im}(p) \tag{18}$$

The interpolation of the GAF matrix ($\mathbf{Q}_{hh}(k)$) is accomplished by a so called Special Linear Interpolation (SLI). I.e., the GAF matrix is interpolated with respect to the reduced frequency $k$ by a cubic radial basis function. The real and imaginary parts are treated separately, where the imaginary part is divided by the reduced frequency before interpolation, to match closely the terms in equation (17). This iteration is repeated for a range of flight velocities resulting in a set of unsorted converged eigenvalues, representing damping and frequencies of the aeroelastic coupled system. When the real part of the eigenvalue becomes positive, flutter occurs. The converged eigenvalues are subsequently tracked and sorted using the Hungarian-method by James Munkres to handle potential mode crossings.

## B. $p$ Method

To avoid the iterations due to the disparity between the values $p$ and $k$ in eq.(18), the so called $p$ method was proposed [27]. The transfer functions of the aerodynamic GAF matrix can be approximated by rational functions, e.g. by Roger's method [28]. With the analytical Laplace transform for rational functions, the GAF matrix can be expressed as an improper state space model by analytical continuation.

$$\mathbf{Q}_{hh}(\hat{s}) = \mathbf{Q^0}_{hh} + \mathbf{Q^1}_{hh}\, \hat{s} + \mathbf{Q^2}_{hh}\, \hat{s}^2 + \mathbf{D}\left(\hat{s}\mathbf{I} - \mathbf{R}\right)^{-1} \mathbf{E}\hat{s} \tag{19}$$

The variable $\hat{s}$ is the Laplace equivalent to the reduced frequency $k$.

$$ik = i\omega \left(\frac{c_{\text{ref}}/2}{V}\right) \Leftrightarrow \hat{s} = s\left(\frac{c_{\text{ref}}/2}{V}\right) \tag{20}$$

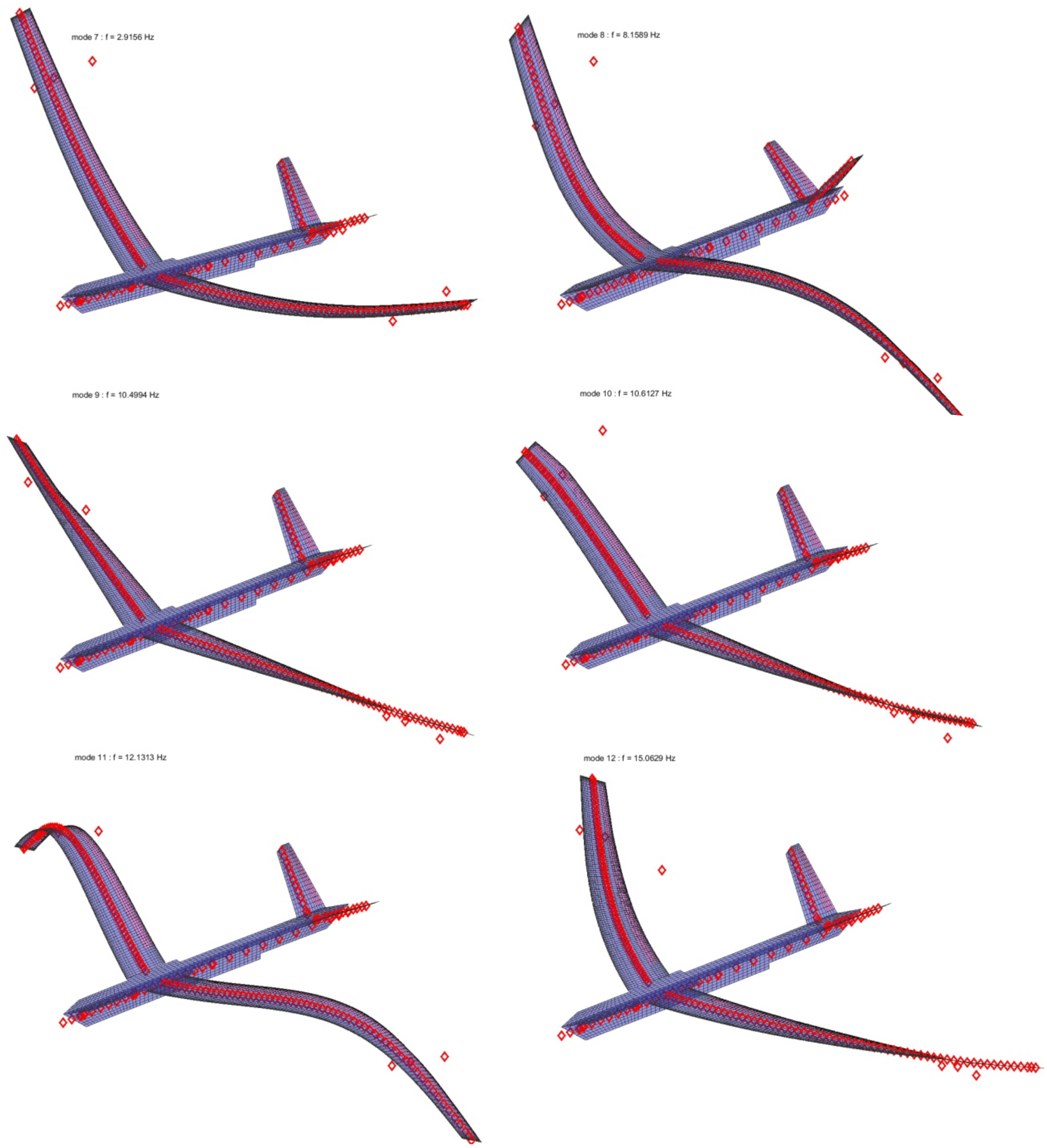


**Figure 1. modeshapes**

With this relationship, the equations of motion can then be expressed in the Laplace domain.

$$\left[\mathbf{M}_{hh}\, s^2 + \mathbf{B}_{hh}\, s + \mathbf{K}_{hh} - q_\infty \mathbf{Q}_{hh}(\hat{s})\right] \mathbf{u_h} = 0. \tag{21}$$

Eq. (21) is then cast as a first order ODE in a state space system, where the eigenvalues of the system matrix can be determined directly. This method has its root in control theory and was applied to analyze control laws for an Active Flutter Suppression system [27]. Again, this procedure is repeated for a range of velocities and the modes are tracked by the Hungarian method.

### C. Linearization of non-linear integrated model

An alternative to the $p$-method is the linearization of an integrated non-linear model of the flexible aircraft. Instead of setting up the system matrix of a linear state space system directly, the equations of motion for a flexible free flying aircraft with unsteady aerodynamic effects are formulated as a nonlinear system. The approach is detailed in reference [9] and not repeated here. It features a equations of motion based on mean axes constraints, i.e. with nonlinear rigid body motion equivalent to Newton-Euler and linear structural dynamics. The unsteady aerodynamics are fitted by a ”physical” rational function approximation, i.e. before multiplication with the differentiation matrices. This way quasi-steady aerodynamics can be separated from unsteady effects and therefore corrected independently. After a trimming procedure, the model is linearized and the eigenvalues of the system can be determined accordingly. Additional effects, such as linearized direction of gravity, nonlinear drag polar etc. can be accounted for in a straight forward way. As the described modelling scheme also relies on a RFA, it can be considered a special case of the $p$-method. This approach is used to generate the linear models for controller synthesis after some additional model order reduction techniques are applied.

### D. Flutter Analysis of the Demonstrator Aircraft

The flutter analysis for the demonstrator aircraft has been obtained by linearization of the non-linear integrated model [7] after updating the structural properties with ground test data [23]. The results in the present paper reflect some recent updates in terms of structural properties and modelling. The aerodynamic grid for the nominal model is with a cruciform shaped fuselage as shown in figure 1 for the mode shape illustration. The standard DLM was used to determine the unsteady aerodynamics.

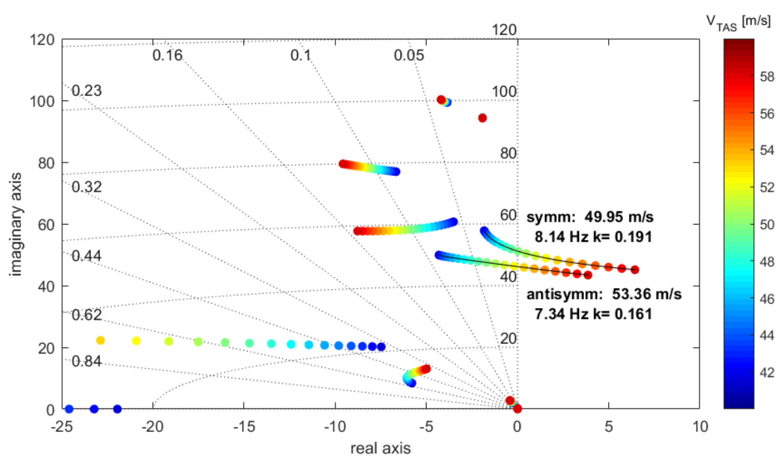


**Figure 2. flutter poles**

Figure 2 shows the pole migration when increasing the true airspeed at sea level. Two aeroelastic modes cross the imaginary axis and become unstable. The first symmetric flutter mode at 49.95 m/s with a frequency of 8.14 Hz. The second flutter mode is antisymmetric at 53.36 m/s with a frequency of 7.34 Hz. The classical flutter V-f and V-g plots are depicted in figure 3. The reduced frequencies at which flutter occurs are k=0.191 and k=0.161, respectively.

Finally, looking at at the two flutter modes and their respective modal contributions. For the first symmetric flutter mode the main contributions are the first symmetric wing bending (mode 7) and first wing torsion (mode 9) with a noticeable contribution of the symmetric second wing bending (mode 11). The symmetric first in-plane bending mode (mode 12) only has a minor contribution to the first flutter mode.

The second flutter mode is antisymmetric and has main contributions from the first antisymmetric wing bending (mode 8) and torsion (mode 10).

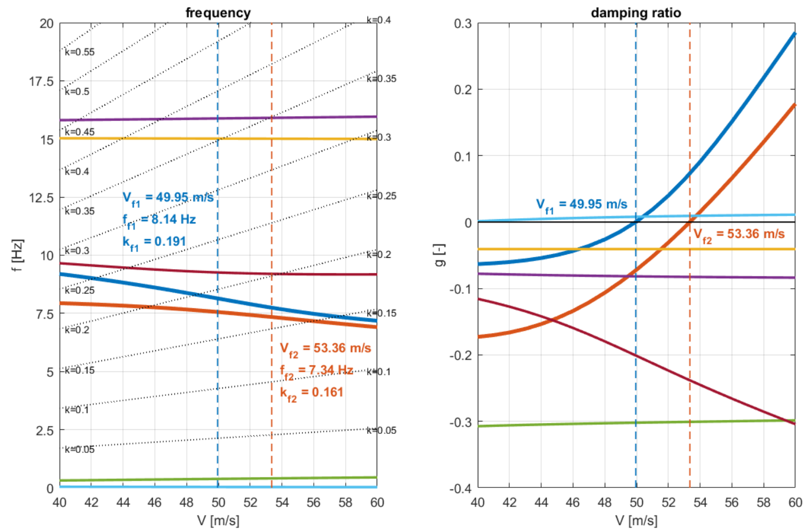


**Figure 3. V-g / V-f diagram**

**Table 2. contribution of the structural modes to the flutter modes**

| **structural mode no.** | **description of structural mode** | **modal contribution [%]** | |
|---|---|---|---|
| | | *symmetric flutter mode 1* | *antisymmetric flutter mode 2* |
| | | $V_{f1} = 49.95\,\mathrm{m/s}$ | $V_{f2} = 53.36\,\mathrm{m/s}$ |
| | | $f_{f1} = 8.14\,\mathrm{Hz}$ | $f_{f2} = 7.34\,\mathrm{Hz}$ |
| 7 | symmetric – 1st wing bending | **47.1** | 1.0 |
| 8 | antisymmetric – 1st wing bending | 0.5 | **51.2** |
| 9 | symmetric – 1st wing torsion | **34.7** | 1.9 |
| 10 | antisymmetric – 1st wing torsion | 1.2 | **37.5** |
| 11 | symmetric – 2nd wing bending | **12.3** | 0.4 |
| 12 | symmetric – 1st wing in-plane bending | 2.2 | 0.1 |

### E. Flutter Solution for different Aerodynamic Methods and Models

After examination of the nominal flutter results, the question arises how the different aerodynamic methods and modelling strategies for the fuselage affect the flutter results. The methods that are compared is the standard DLM and an enhanced DLM method (eDLM), accounting for direction of lift using the appropriate boundary condition matrices. The 3D panel method model was not considered since it reflects an old status and would not provide insights regarding a pure comparison of the methods.

Four different aerodynamic panel grids were used for the present study. An aerodynamic model with thin lifting surfaces for the wings without consideration of the fuselage (model 1), a grid with a fuselage modelled by cruciform shaped lifting surfaces (model 2) and a grid where the fuselage is modelled by quadrilateral source panels (model 3). The first three models represent the wing and tail by thin mean lifting surfaces. The same discretizations are applied to the DLM and enhanced eDLM method. Except for model 3, since the use of non-lifting body source panels already require a treatment of on-flow conditions in the x-direction, hence the standard DLM is not applicable. The fourth model is an aerodynamic grid which models the surface contour of the wings for a velocity potential based 3D panel method (model 4). This model is not included in the comparison, since an older status of the geometry was used. The aerodynamic grid are depicted in figure 4.

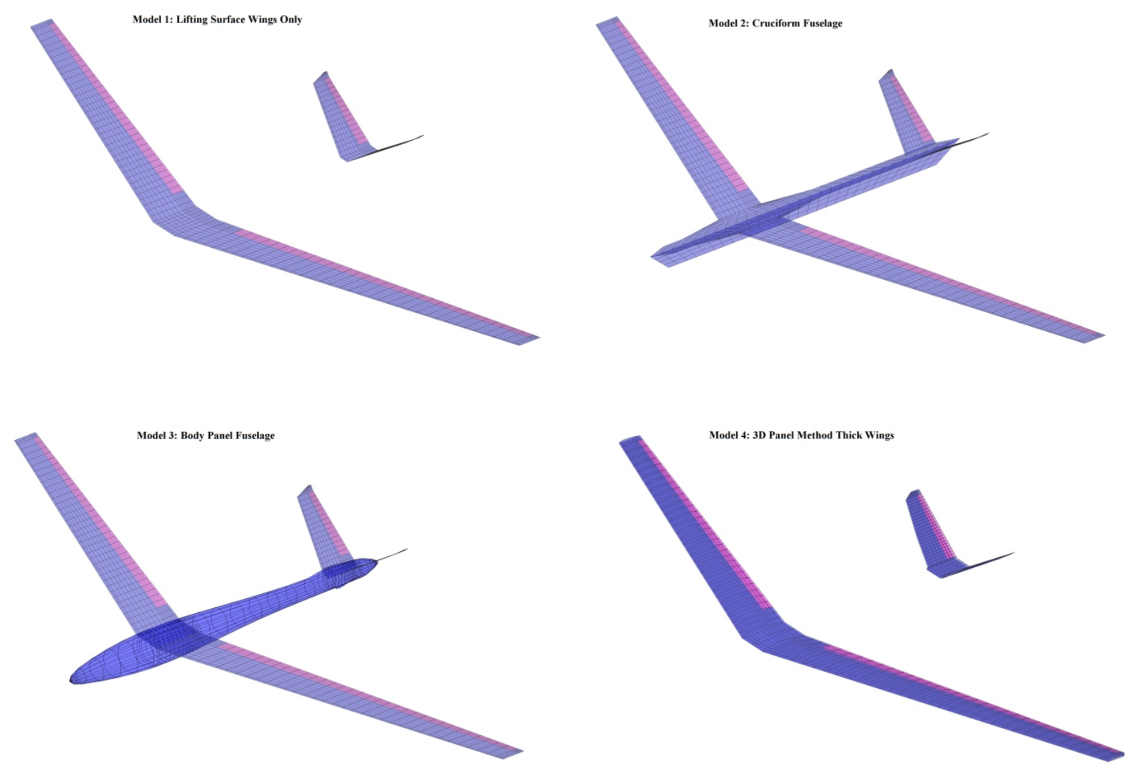


**Figure 4. Aerodynamic grids: Lifting Surface Wings Only (Model 1), With Cruciform Fuselage (Model 2), With Body Panel Fuselage (Model 2) and 3D panel Method Thick Wings (Model 4)**

The Aerodynamic Influence Coefficient Matrices have been calculated for ten reduced frequencies $k = 0.0$, 0.001, 0.05, 0.1, 0.2, 0.5, 1.0, 1.5, 2.0 and 3.5. The Generalized Forces are generated with the structural modeshapes and the respective boundary condition matrices for the standard DLM and the enhanced eDLM. The flutter results have been obtained with the $p - k$ method and the $p$ method. For the $p$-method, the GAF matrices were fitted with a Rational Function Approximation according to Roger's Method using eight poles with a standard distribution.

The flutter results of the various aerodynamic grids, aerodynamic methods and flutter methods are summarized in table 3.

Barely any difference are noticeable in the results, since the flutter modes are dominated by out of plane motion. The fuselage modelling has no influence on the results, as no fuselage modes are participating in the flutter mechanism.

Also, the differences between the $p$ and $p - k$ method are insignificant and stem from the different evaluation methods for the GAFs with respect to the reduced frequency. The RFA for the $p$ method is a regression model over the entire range of reduced frequencies $k$, while the special linear interpolation is a interpolation method based on radial functions. The interpolation method is exact for the underlying computed reduced frequency, while the regression model is the best fit in a least square sense over the entire range of reduced frequencies.

The eDLM shows a slightly higher flutter speed and slightly lower frequency for the first flutter mode. The modal participation in table 2 showed a minor contribution of the in-plane bending mode (mode 12), which is likely the cause for the minimal differences between the DLM and eDLM results.

**Table 3. Flutter Results**

| **Flutter Mode** | **Model 1: wings only** | | | | **Model 2: cruciform fuselage** | | | | **Model 3: body panels** | |
|---|---|---|---|---|---|---|---|---|---|---|
| | DLM | | eDLM | | DLM | | eDLM | | eDLM | |
| | $p$ | $pk$ | $p$ | $pk$ | $p$ | $pk$ | $p$ | $pk$ | $p$ | $pk$ |
| **symmetric** | | | | | | | | | | |
| $V_{f1}$ [m/s] | 48.95 | 48.90 | 50.14 | 50.07 | 48.79 | 48.74 | 50.14 | 50.07 | 49.99 | 49.92 |
| $f_{f1}$ [Hz] | 8.30 | 8.29 | 8.21 | 8.22 | 8.31 | 8.31 | 8.21 | 8.22 | 8.23 | 8.23 |
| $k_{f1}$ [-] | 0.199 | 0.199 | 0.192 | 0.192 | 0.200 | 0.200 | 0.192 | 0.192 | 0.193 | 0.193 |
| **antisymmetric** | | | | | | | | | | |
| $V_{f2}$ [m/s] | 53.09 | 53.10 | 53.54 | 53.55 | 53.10 | 53.11 | 53.56 | 53.57 | 53.52 | 53.53 |
| $f_{f2}$ [Hz] | 7.42 | 7.42 | 7.43 | 7.43 | 7.42 | 7.43 | 7.43 | 7.43 | 7.43 | 7.43 |
| $k_{f2}$ [-] | 0.164 | 0.164 | 0.163 | 0.163 | 0.164 | 0.164 | 0.163 | 0.163 | 0.163 | 0.163 |

# V. Generalized Aerodynamic Forces of the Flutter Demonstrator

While no significant changes in the flutter results were observed, a scrutinizing look at the Generalized Aerodynamic Forces is warranted to assess the differences among the various aerodynamic methods. The AICs are determined for the three different aerodynamic grids with its different modelling strategies for the fuselage. The grids are evaluated using the standard DLM and the enhanced DLM, except for the body panel fuselage model, where only the eDLM was used. The reduced frequencies used for plotting are $k_{\text{red}} = 0.0$, 0.001, 0.05, 0.1, 0.2, 0.5, 1.0, 1.5 and 2.0.

At first, the flutter GAFs including the cross coupling terms for the two relevant flutter mechanisms will be examined. Then the aerodynamic forcing for the in-plane wing bending mode is looked at. The differences in fuselage modelling is most relevant for the vertical and lateral rigid body modes. And finally some results from the 3D panel Method are investigated, although not completely comparable, as the panel model represents an older status of the geometry.

## A. Flutter GAFs

The modes participating in the two flutter modes are 7, 9 and 11 for the symmetric, respectively 8 and 10 for the antisymmetric flutter mode. The flutter results, summarized in table 3 showed hardly any difference between the aerodynamic methods and fuselage modelling approaches. This is not surprising as the flutter mechanisms are driven almost solely by out of plane modes, which are captured well by the standard DLM.

Figure 5 shows the elements 7, 9 and 11 of the GAF matrix $\mathbf{Q}_{hh}$ for the symmetric flutter mode including the cross couplings.

Correspondingly, figure 9 shows the elements 8 and 10 of the GAF matrix $\mathbf{Q}_{hh}$ for the antisymmetric flutter mode.

The matrix elements of $\mathbf{Q}_{hh}$ for the flutter relevant structural modes are hardly influenced by the aerodynamic method used. Hence, the flutter results are affected only insignificantly. Also note that within the project FLEXOP, Rozov [29] generated results using an frequency domain linearized Euler CFD code. The results for the GAFs compare visually well. Attention needs to be paid because different reduced frequencies were used in the corresponding plots.

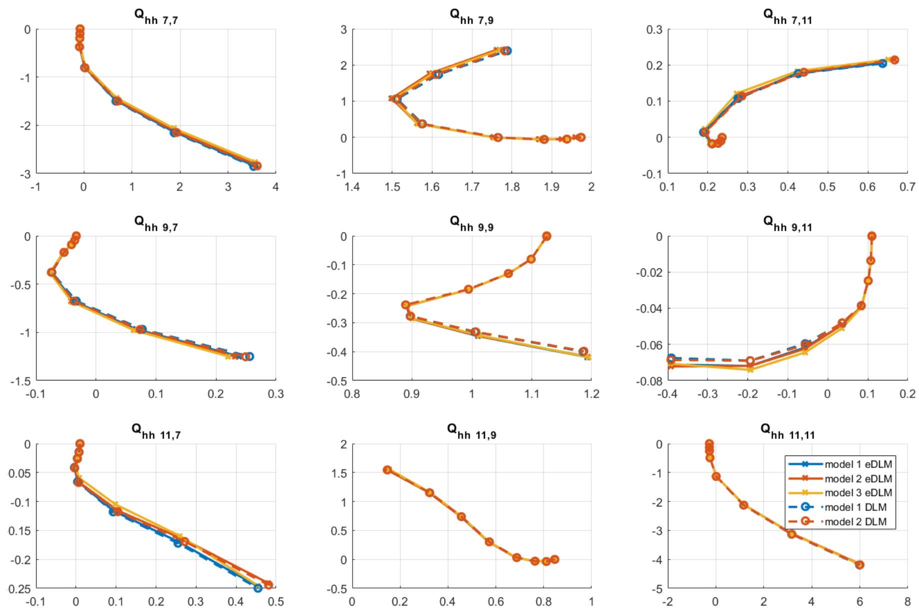


**Figure 5. Generalized Aerodynamic Force Matrix $Q_{hh}$ for the symmetric flutter mode. Elements 7-9-11 including cross couplings**

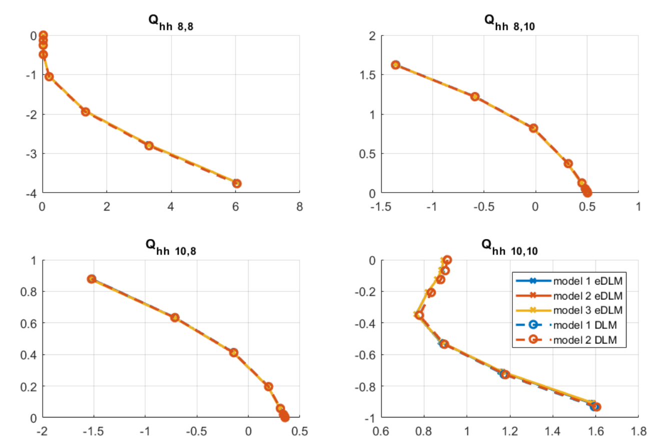


**Figure 6. Generalized Aerodynamic Force Matrix $Q_{hh}$ for the symmetric flutter mode. Elements 8-10 including cross couplings**

## B. In-plane Bending Mode

The most differences between the standard DLM and the enhanced eDLM are expected for modes where large in-plane motion is experienced. This is the case for the first symmetric in-plane bending mode number 12. Albeit, this mode is not participating in the flutter mechanism, the in-plane aerodynamic forces are of interest as they can not be modelled accurately by the classic DLM, since it does not account for the effect of the increased onflow velocity. It merely models the changed circulation due to normalwash at the control point of the box. A pure in-plane motion therefore does not induce any aerodynamic loading. The enhanced eDLM correctly reflects the onflow condition at the quarter chord point by considering the motion induced velocities via the boundary condition matrices.

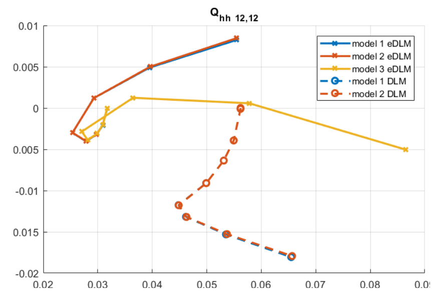


**Figure 7. $\mathbf{Q}_{hh}$ element for the 1st symmetric in-plane bending mode number 12**

When inspecting the The GAF matrix $\mathbf{Q}_{hh}$ for the in first plane bending mode in figure 7, the differences between the standard DLM (dashed lines) and the enhanced version (solid lines) are obvious. The results are unaffected by the aerodynamic grids with a cruciform shaped fuselage (model 2) and wings only (model 1), for both the standard DLM and the eDLM. The in-plane motion of the unloaded cruciform fuselage does not induce additional aerodynamic forces. Only the body panel fuselage shows a different behavior for higher reduced frequencies, as the body panels displace the flow around the fuselage.

The differences in aerodynamic forces for in-plane motion urge for caution when flutter mechanisms are considered where in plane modes are participating. This the case e.g. for T-tail flutter.

## C. Fuselage Modes

Next consideration is the influence of the modelling strategies for the fuselage. The differences are most pertinent for the rigid body heaving (mode 3) and swaying (mode 2), as well as the pitching (mode 5) and yawing (mode 6) motion. Figure 8 shows the respective Generalized Aerodynamic Forces.

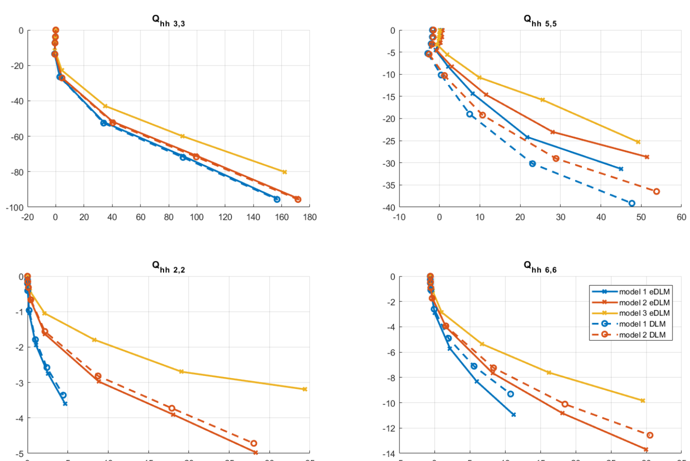


**Figure 8. Generalized Aerodynamic Forces for the vertical and lateral rigid body fuselage modes**

The lateral swaying shows the effects very clearly. For the vertical heaving, the wing has a large influence. The difference between standard and enhance DLM are not as relevant. The body panel model shows a more pronounced influence, suggesting that the effects are underestimated, when a cruciform fuselage model is chosen.

### D. 3D panel method

Finally, the GAFs for the 3D panel model (model 4) are compared to the various DLM models for the antisymmetric flutter mode.

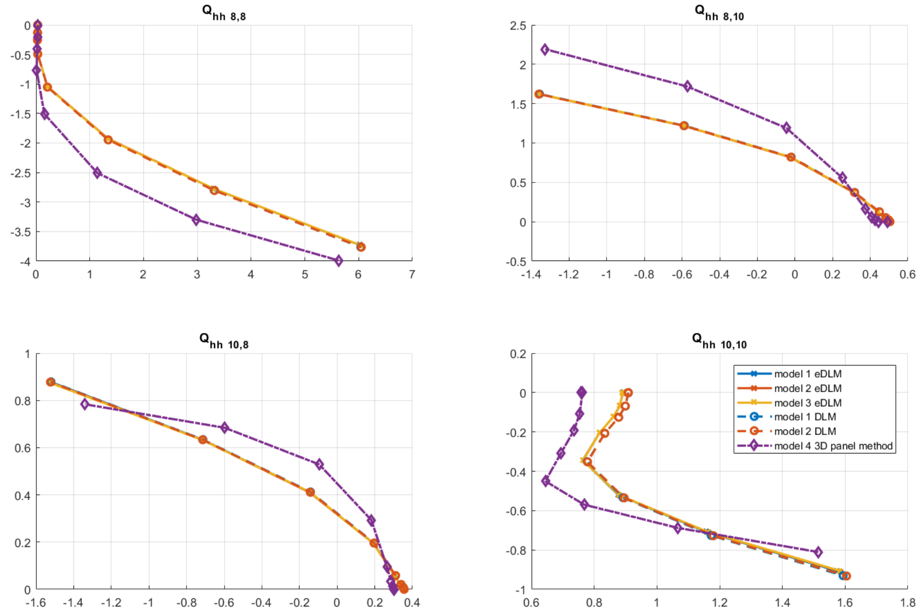


**Figure 9. GAFs of the 3D Panel Method for the symmetric flutter mode**

The overall behavior looks similar to the DLM results, however there are noticeable differences. These might stem from a slightly different geometry corresponding to an older status of the aircraft data. When comparing the trajectories in the complex plane qualitatively comparing with the results of Rozov [29], similar trends are observable. Further research with an updated 3D panel model needs to be conducted. Furthermore, the 3D panel methods should include a body panel fuselage model as well, to fully exploit its potential.

## VI. Summary and Conclusions

Flutter analyses with different potential flow based aerodynamics have been compared for a subscale demonstrator aircraft that was specifically designed to experience a flutter behavior within the flight envelope.

Particular focus was placed on the in-plane forces, which are not captured at all by the standard Doublet Lattice Method. Therefore, an enhanced DLM was employed, using a cross product Kutta Joukowsky Law to recover directional lift components at box level following an approach proposed by van Zyl [16].

Another aspect covered is the modelling strategy for the fuselage. Three aerodynamic grids have been set up, one where only the lifting surfaces were modelled, the second with a cruciform shaped fuselage, where the projected area is modelled by lifting surfaces and a third model which uses quadrilateral unsteady source panels to model the fuselage as a nonlifting body.

The flutter results obtained with the investigted aerodynamic methods were compared to a nominal model presented in [7] following a integrated modelling approach for flexible aircraft with nonlinear flight mechanics introduced in [9]. The flutter analysis for the nominal model were obtained by linearization of the nonlinear model. The results for the present study on the potential flow methods have been obtained by the classical $p-k$ and $p$ method. The latter requires a Rational Function Approximation of the generalized aerodynamic force matrix $\mathbf{Q}_{hh}$.

The symmetric and antisymmetric flutter modes showed no significant differences neither between the different aerodynamic methods, nor to the nominal model. This is not surprising as the standard DLM is able to capture out of plane modes very well, which contribute almost exclusively to the flutter mechanisms at hand. The GAF elements associated with the flutter modes are almost identical.

The most striking differences show in the aerodynamic transfer function of the first in-plane bending structural mode (mode 12). The standard DLM can not account for forces in x- direction and does not account for motion induced velocities due to the in-plane movement of the wing. As expected the standard and the enhanced DLM show completely different behavior. For higher reduced frequencies also the body panels and the displaced flow about the fuselage seems to have a bigger influence. However, since this mode is not participating in the symmetric and antisymmetric mechanisms, the flutter results are unaffected.

Next, the GAFs for the rigid body modes were investigated. The vertical and lateral heaving (heave and sway mode) showed a clear influence of the fuselage modelling. The cruciform shaped fuselage still seems to underestimate the forcing effects compared to the body panel model. The effects are more clearly visible for the lateral modes, as damping due to the wing surface does not contribute in that case.

Finally, a fourth model was examined, an unsteady 3D panel method based on the velocity potential which models the surface contour of the wing. By pressure integration along this surface contour, the forces are recovered also in in-plane direction. The model still represented an old status of the geometry and modal data and can hence not be directly compared to the other flutter results. Nevertheless, the GAFs for the antisymmetric flutter mode were plotted and show a similar behavior. Further investigations with an updated model will be conducted in the future.

Although the flutter behavior is mostly unaffected by the different aerodynamic methods and grids in the present study, caution is warranted. A Ground Vibration Test (GVT) [30] showed a low frequency in plane mode associated with the mounting of the wings. This mode is not reflected in the current Finite Element Model. As the in-plane mode is close in frequency to the ones participating in the flutter mechanisms, this study should be repeated with an FE model updated to the most recent modal data.

## Acknowledgements

The research leading to these results is part of the FLiPASED project. This project has received funding from the European Unions Horizon 2020 research and innovation program under grant agreement No. 815058.

## References

[1] Kier, T., "An Integral Flexible Aircraft Model for Optimal Control Surface Scheduling of Manoeuvre Load Alleviation and Wing Shape Control Functions," *International Forum on Aeroelasticity and Structural Dynamics, 13-17 June 2022, Madrid, Spain*, No. IFASD-2022-093, 2022.

[2] Wüstenhagen, M., "Model Selection for a Multiple-Model Adaptive Gust Load Alleviation Controller," *International Forum on Aeroelasticity and Structural Dynamics, 13-17 June 2022, Madrid, Spain*, No. IFASD-2022-136, 2022.

[3] Pusch, M., Kier, T. M., Tang, M., Dillinger, J. K., and Ossmann, D., "Advanced Gust Load Alleviation using Dynamic Control Allocation," *AIAA SCITECH 2022 Forum*, American Institute of Aeronautics and Astronautics, jan 2022.

[4] Burlion, L., Poussot-Vassal, C., Vuillemin, P., Leitner, M., and Kier, T., "Longitudinal Manoeuvre Load Control of a Flexible Large-Scale Aircraft," *19th IFAC World Congress, Cape Town, South Africa*, 2014, pp. 3413–3418.

[5] Pusch, M., Ossmann, D., and Luspay, T., "Structured Control Design for a Highly Flexible Flutter Demonstrator," *Aerospace*, Vol. 6, No. 3, mar 2019, pp. 27.

[6] Bartasevicius, J., Koeberle, S. J., Teubl, D., Roessler, C., and Hornung, M., "Flight Testing of 65kg T-FLEX Subscale Demonstrator," *32nd Congress of the International Council of the Aeronautical Sciences (ICAS2021), 6.-10. Sept. 2021, Shanghai, China*, No. ICAS 2020-0707, ICAS, 2021.

[7] Wüstenhagen, M., Kier, T., Meddaikar, Y. M., Pusch, M., Ossmann, D., and Hermanutz, A., "Aeroservoelastic Modeling and Analysis of a Highly Flexible Flutter Demonstrator," *2018 Atmospheric Flight Mechanics Conference*, American Institute of Aeronautics and Astronautics, jun 2018.

[8] Kier, T., Looye, G., Scharpenberg, M., and Reijerkerk, M., "Process, Methods and Tools for Flexible Aircraft Flight Dynamics Model Integration," *International Forum on Aeroelasticity and Structural Dynamics*, No. IF-060, CEAS/AIAA, 2007.

[9] Kier, T. M. and Looye, G. H. N., "Unifying Manoeuvre and Gust Loads Analysis," *International Forum on Aeroelasticity and Structural Dynamics*, No. IFASD-2009-106, 2009.

[10] Luspay, T., Ossmann, D., Wuestenhagen, M., Teubl, D., Baár, T., Pusch, M., Kier, T. M., Waitman, S., Ianelli, A., Marcos, A., Vanek, B., and Lowenberg, M. H., "Flight control design for a highly flexible flutter demonstrator," *AIAA Scitech 2019 Forum*, American Institute of Aeronautics and Astronautics, jan 2019.

[11] Takarics, B., Patartics, B., Luspay, T., Vanek, B., Roessler, C., Bartasevicius, J., Koeberle, S. J., Hornung, M., Teubl, D., Pusch, M., Wüstenhagen, M., Kier, T. M., Looye, G., Bauer, P., Meddaikar, Y. M., Waitman, S., and Marcos, A., "Active Flutter Mitigation Testing on the FLEXOP Demonstrator Aircraft," *AIAA Scitech 2020 Forum*, No. AIAA 2020-1970, American Institute of Aeronautics and Astronautics, jan 2020.

[12] Albano, E. and Rodden, W., "A Doublet-Lattice Method for Calculating Lift Distributions on Oscillating Surfaces in Subsonic Flows," *AIAA Journal*, Vol. 7, No. 2, 1969, pp. 279–285.

[13] Kalman, T. P., Rodden, W. P., and Giesing, J. P., "Application of the Doublet-Lattice Method to Nonplanar Configurations in Subsonic Flow," *Journal of Aircraft*, Vol. 8, No. 6, 1971, pp. 406–413.

[14] Rodden, W., Taylor, P., and Jr., S. M., "Further Refinement of the Subsonic Doublet-Lattice Method," *Journal of Aircraft*, Vol. 9, No. 10, 1998, pp. 693–702.

[15] van Zyl, L. H., "Unsteady Panel Method for Complex Configurations Including Wake Modeling," *Journal of Aircraft*, Vol. 45, No. 1, 2008, pp. 276–285.

[16] van Zyl, L. H. and Mathews, E. H., "Aeroelastic Analysis of T-Tails Using an Enhanced Doublet Lattice Method," *Journal of Aircraft*, Vol. 48, No. 3, 2011, pp. 823–831.

[17] Fiddes, S. P., Burkett, C. W., and Kier, T. M., "An Advanced Panel Method for Compressible Subsonic Unsteady Flow Past Complex Geometries," *International Forum on Aeroelasticity and Structural Dynamics*, No. IFASD-2015-181, 2015.

[18] Kier, T. M., Verveld, M. J., and Burkett, C. W., "Integrated Flexible Dynamic Loads Models Based on Aerodynamic Influence Coefficients of a 3D Panel Method," *International Forum on Aeroelasticity and Structural Dynamics*, No. IFASD-2015-179, 2015.

[19] Göthert, B., "Ebene und räumliche Strömung bei hohen Unterschallgeschwindigkeiten: Erweiterung der Prandtl'schen Regel," Tech. Rep. Bericht 127, Lilienthal Gessellschaft, 1940.

[20] Pistolesi, E., "Betrachtungen über die gegenseitige Beeinflussung von Tragflügelsystemen," *Gesammelte Vorträge der Hauptversammlung 1937 der Lilienthal Gesellschaft*, 1937.

[21] Rodden, W., Giesing, J., and Kalman, T., "New Developments and Applications of the Subsonic Doublet-Lattice Method for Nonplanar Configurations," *AGARD Symposium on unsteady aerodynamics for aeroelastic analyses of interfering surfaces*, No. AGARD-CP-80-71, AGARD, 1971.

[22] Kirkup, S., *The Boundary Element Method in Acoustics*, Vol. 8, 01 2007.

[23] Meddaikar, Y. M., Dillinger, J., Klimmek, T., Krüger, W., Wüstenhagen, M., Kier, T. M., Hermanutz, A., Hornung, M., Rozov, V., Breitsamter, C., Alderman, J., Takarics, B., and Vanek, B., "Aircraft Aeroservoelastic Modelling of the FLEXOP Unmanned Flying Demonstrator," *AIAA Scitech 2019 Forum*, American Institute of Aeronautics and Astronautics, jan 2019.

[24] Guyan, R. J., "Reduction of stiffness and mass matrices," *Journal of Aircraft*, Vol. 3, No. 2, 1965, pp. 380.

[25] Hassig, H. J., "An Approximate True Damping Solution of the Flutter Equation by Determinant Iteration," *Journal of Aircraft*, Vol. 8, No. 11, 1971, pp. 885–889.

[26] Rodden, W. P., Harder, R. L., and Bellinger, E. D., "Aeroelastic Addition to NASTRAN," Tech. Rep. NASA CR-3094, NASA, March 1979.

[27] Abel, I., "An analytical technique for predicting the characteristics of a flexible wing equipped with an active flutter-suppression system and comparison with wind-tunnel data," Tech. Rep. NASA TP-1367, NASA LARC, 1979.

[28] Roger, K. L., "Airplane Math Modeling Methods for Active Control Design," *AGARD Structures and Materials Panel*, No. AGARD/CP-228, AGARD, April 1977, pp. 4–1 – 4–11.

[29] Rozov, V., Volmering, A., Hermanutz, A., Hornung, M., and Breitsamter, C., "CFD-Based Aeroelastic Sensitivity Study of a Low-Speed Flutter Demonstrator," *Aerospace*, Vol. 6, No. 3, mar 2019, pp. 30.

[30] Sodja, J., Breuker, R. D., Meddaikar, Y. M., Dillinger, J. K., Soal, K., Govers, Y., Krueger, W., Georgopoulos, P., Koimtzoglou, C., Roessler, C., Koeberle, S. J., Bartasevicius, J., Teubl, D., Gyulai, L., Toth, S., Nagy, M., Balogh, D., Jasdi, M., Bauer, P., and Vanek, B., "Ground Testing of the FLEXOP Demonstrator Aircraft," *AIAA Scitech 2020 Forum*, American Institute of Aeronautics and Astronautics, jan 2020.